JACS
JOURNAL OF THE AMERICAN CHEMICAL SOCIETY

Article

pubs.acs.org/JACS

# Folding of Oligoviologens Induced by Radical−Radical Interactions

Yuping Wang,[†] Marco Frasconi,[†] Wei-Guang Liu,[‡] Zhichang Liu,[†] Amy A. Sarjeant,[†] Majed S. Nassar,[§] Youssry Y. Botros,[§,⊥] William A. Goddard, III,[‡] and J. Fraser Stoddart*[,†]

[†]Department of Chemistry, Northwestern University, 2145 Sheridan Road, Evanston, Illinois 60208, United States

[‡]Materials and Process Simulation Center, California Institute of Technology, 1200 East California Boulevard, Pasadena, California 91125, United States

[§]Joint Center of Excellence in Integrated Nano-Systems (JCIN), King Abdul-Aziz City for Science and Technology (KACST), P.O. Box 6086, Riyadh 11442, Saudi Arabia

[⊥]University Research Office, Intel Corporation, Building RNB-6-61, 2200 Mission College Boulevard, Santa Clara, California 95054, United States

Supporting Information

**ABSTRACT:** We report the synthesis of a series of homologous oligoviologens in which different numbers of 4,4′-bipyridinium ($BIPY^{2+}$) subunits are linked by *p*-xylylene bridges, as a prelude to investigating how their radical cationic forms self-assemble both in solution and in the solid state. The strong radical−radical interactions between the radical cationic forms of the $BIPY^{2+}$ units—namely, $BIPY^{\bullet+}$—in these oligoviologens induce intra- or intermolecular folding of these homologues. UV/Vis/NIR spectroscopic studies and DFT quantum mechanics indicate that the folding of the shorter oligoviologens is dominated by intermolecular radical−radical interactions. In addition to intermolecular interactions, strong intramolecular radical−radical interactions, which give rise to an NIR absorption band at 900 nm, tend to play a crucial role in governing the folding of the longer oligoviologens. The solid-state superstructure of the oligoviologen with three $BIPY^{2+}$ units reveals that two intertwining chains fold together to form a dimer, stabilized by intermolecular radical−radical interactions. These dimers continue to stack in an infinite column through intermolecular radical−radical interactions between them. This research features an artificial biomimetic system which sustains delicate secondary and tertiary structures, reminiscent of those present in nucleic acids and proteins.

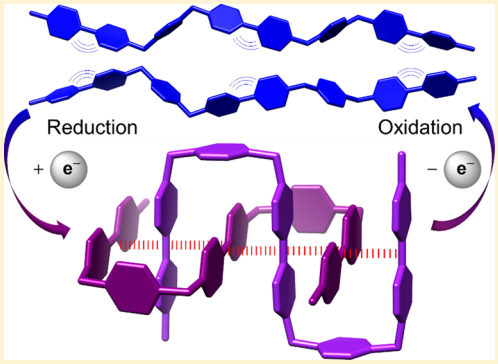


## INTRODUCTION

Biomolecules achieve most of their functions, such as molecular recognition, catalysis, and information storage, not only by folding into specific compact secondary and tertiary structures in a well-organized and complex manner, but also by switching conformations reversibly among different states in response to various stimuli and conditions. By constructing a vast amount of highly hierarchical superstructures from only three major building blocks—namely, proteins, nucleic acids, and polysaccharides—nature teaches us vividly how noncovalent bonding interactions play a crucial role in molecular recognition processes.[1] In general, intermolecular interactions, in concert with intramolecular forces, control the assembly of biological systems.[2] Although intermolecular interactions are probably more prevalent in biosystems,[3] such as the hybridization of DNA single strands which rests on the interactions between two complementary strands, intramolecular interactions[4] are also not unimportant since the secondary structures of polypeptides rely, for the most part, on various interactions of this type. More significantly, intramolecular interactions between $\alpha$-amino acid side chains[5] that project at well-defined geometrical positions from $\beta$-strands, turns, and helical subunits[4,6] help drive the formation of the tertiary structures of many proteins. Thus, achieving a better understanding of the cooperative and competitive relationships between intra- and intermolecular interactions could not only (i) pave the way for unraveling the secrets of life but also (ii) lead to the syntheses and characterization of abiotic counterparts to nature's biomacromolecules.

In order to address these challenges, a large variety of compounds[7] have been designed and synthesized on the basis of inspiration gained from the behavior of biomacromolecules. Among these artificial biomimetic compounds, foldamers[8] have been singled out as promising candidates and have attracted increasing attention in recent decades. Constructed under the mantle of noncovalent bonding interactions,[1] foldamers can achieve[9] precise, yet reversible, control over structural organization, opening up the possibility of fulfilling functions even beyond the reach of biomacromolecules. Precise control of intra- and intermolecular interactions, however, remains an important goal to achieve in the case of foldamers.[5−9] Typically,

**Received:** October 29, 2014
**Published:** December 10, 2014





DOI: 10.1021/ja5111305
J. Am. Chem. Soc. 2015, 137, 876−885

the switching processes between unfolded and folded (co)-conformations, especially the helical folding (co)-conformations with characteristic molecular recognition properties and complex chiralities, involve changes in solvent composition[10] and temperature,[11] as well as other alternative external stimuli such as pH,[12] ions,[13] and light.[14]

In spite of the fact that the radical chemistry of compounds containing 1,1′-dialkyl-4,4′-bipyridinium ($BIPY^{2+}$) units was well-documented in the early 1960s by Kosower[15] and Hünig,[16] who demonstrated the ability of $BIPY^{\bullet+}$ radical cations to undergo pimerization[17] through radical−radical interactions in water,[18] it is only recently that researchers[19] have started to design systems that take advantage of these kinds of interactions. Indeed, the formation of the radical dimer $[BIPY^{\bullet+}]_2$ can be greatly enhanced in confined environments[20] or by linking viologen derivatives covalently in order to allow[17,21] the optimum overlap of the $\pi$ orbitals between two adjacent viologens. As a result, dendrimers featuring several viologens units in their branches have been shown[22] to shrink upon reduction of the $BIPY^{2+}$ units, with a folding up of their structures resulting in the encapsulation of a fraction of the $BIPY^{\bullet+}$ units within the dendrimer core. Examples of the pimerization of molecules with multiple $BIPY^{\bullet+}$ units within more complex structures, however, are few and far between. Recently, radical cation−$\pi$ interactions have been exploited[23] in the formation of a 1:1 complex between the reduced cyclobis(paraquat-*p*-phenylene) ($CBPQT^{2(\bullet+)}$) ring and a $BIPY^{\bullet+}$ guest under reducing conditions. Upon reducing the electron-deficient $CBPQT^{4+}$, the host diradical dication $CBPQT^{2(\bullet+)}$, composed of two $BIPY^{\bullet+}$ walls and held rigidly at a distance of 7 Å by two *p*-xylylene linkers, can form a stable inclusion complex with methyl viologen radical cation ($MV^{\bullet+}$) guest, characterized[23b] by ideal separations of 3.28 Å between the $BIPY^{\bullet+}$ radical cationic subunits. This radical-stabilized inclusion complex has been employed[24] to template the formation of mechanically interlocked molecules (MIMs) and to generate mechanical motions in the form of translation as well as circumrotation in the context of rotaxanes and catenanes. Herein, we report on (i) the synthesis (Schemes 1 and 2) of a series (Figure 1) of homologous oligoviologens, namely $\mathbf{2V}^{4+}$, $\mathbf{3V}^{6+}$, $\mathbf{4V}^{8+}$, $\mathbf{5V}^{10+}$, and $\mathbf{12V}^{24+}$, and (ii) their characterization by high-resolution mass spectrometry (HRMS) in addition to NMR spectroscopy, before describing (iii) their self-assembly as radical cations, both in solution (iv) by UV/Vis/NIR spectroscopy and cyclic voltammetry (CV) and in the solid state (v) by X-ray crystallography. We also demonstrate that results from computational studies on the folding of these oligoviologens are in good agreement with the experimental data.

**Scheme 1. Synthesis of $3V{\cdot}6PF_6$**

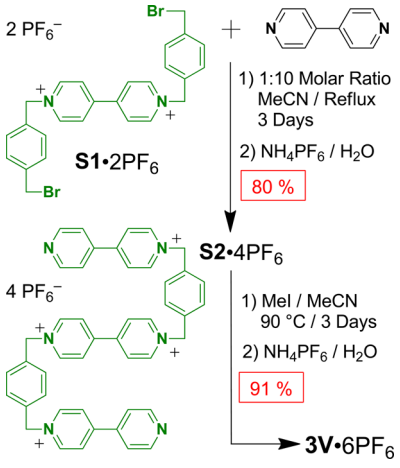


**Scheme 2. Syntheses of $4V{\cdot}8PF_6$ and $12V{\cdot}24PF_6$**

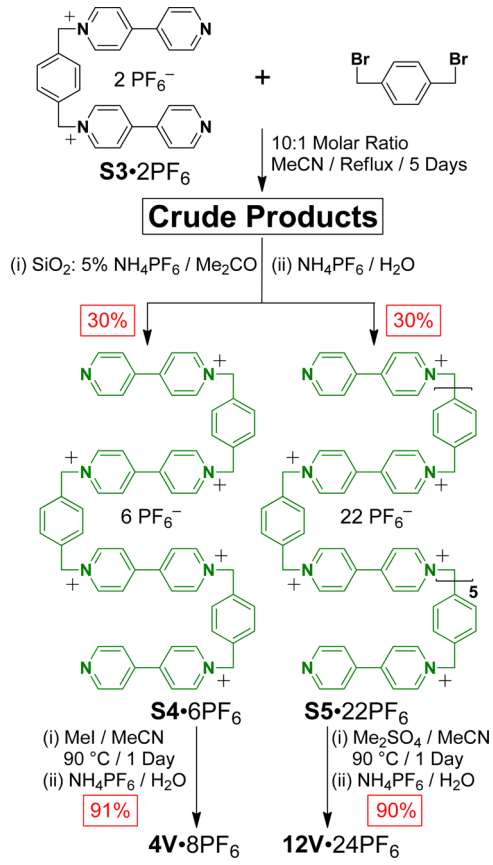


## EXPERIMENTAL SECTION

The full experimental details are provided in the Supporting Information (SI). The most important information is summarized below briefly.

**$S2{\cdot}4PF_6$.** A solution of 4,4′-bipyridine (1.56 g, 10 mmol) in MeCN (40 mL) was added dropwise via syringe at 4 mL·h$^{-1}$ to a refluxing solution of 1,1′-bis(4-(bromomethyl)benzyl)-[4,4′-bipyridine]-1,1′-diium bis(hexafluorophosphate) ($\mathbf{S1}{\cdot}2PF_6$) (814 mg, 1 mmol) in MeCN (40 mL) at 80 °C. After addition, the reaction mixture was stirred for a further 72 h under reflux and then cooled to room temperature. The yellow precipitate was filtered off, washed with $Me_2CO$ and $Et_2O$, and finally purified by column chromatography ($SiO_2$) using 2% $NH_4PF_6$ (m/v) $Me_2CO$ solution as the eluent. The fractions were monitored by mass spectrometry and analytical HPLC. The pure fractions were combined, concentrated under vacuum, re-precipitated in $H_2O$, filtered off, and washed with $H_2O$, MeOH, and finally $Et_2O$ to afford $\mathbf{S2}{\cdot}4PF_6$ as a white crystalline solid (1.01 g, 80%): $^1$H NMR (500 MHz, $CD_3CN$) $\delta$ = 8.97 (d, $J$ = 5.0 Hz, 4H), 8.92 (m, 8H), 8.97 (d, $J$ = 5.0 Hz, 4H), 8.41 (m, 8H), 8.09 (d, $J$ = 5.0 Hz, 4H), 7.60 (s, 8H), 5.87 (s, 4H), 5.87 (s, 4H); $^{13}$C NMR (126 MHz, $CD_3CN$) $\delta$ = 145.4, 134.2, 133.9, 130.0, 130.0, 129.9, 127.2, 126.8, 124.5, 63.6, 63.4; HRMS (ESI) $m/z$ calcd for $C_{46}H_{40}F_{18}N_6P_3$ $[M - PF_6]^+$ 1111.2233, found 1111.2234.

**$3V{\cdot}6PF_6$.** MeI (251 mg, 1.85 mmol) was added dropwise to a solution of $\mathbf{S2}{\cdot}4PF_6$ (125 mg, 0.1 mmol) in DMF (3 mL) with stirring at room temperature. After addition, the mixture was then heated to 90 °C for 72 h and then cooled to room temperature. When $Me_2CO$ was added to the solution, a white precipitate formed immediately.



DOI: 10.1021/ja5111305
J. Am. Chem. Soc. 2015, 137, 876−885

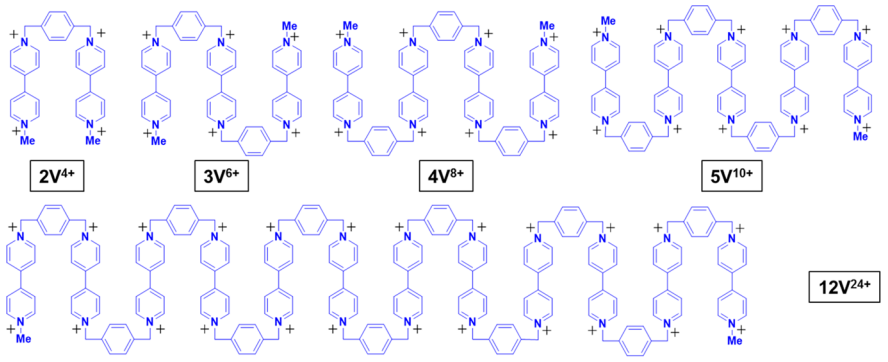


**Figure 1.** Structural formulas of $\mathbf{2V}^{4+}$, $\mathbf{3V}^{6+}$, $\mathbf{4V}^{8+}$, $\mathbf{5V}^{10+}$, and $\mathbf{12V}^{24+}$. The $PF_6^-$ counterions are omitted for the sake of clarity.

The resulting precipitate was filtered off, washed with $Me_2CO$, and re-dissolved in $H_2O$. An excess of $NH_4PF_6$ was added to this solution until no further precipitation was observed. The crude product was filtered off, washed sequentially with $H_2O$, MeOH, and finally $Et_2O$, and dried under vacuum to afford **3V**·6$PF_6$ as a white solid (142 mg, 90%): $^1$H NMR (500 MHz, $CD_3CN$) $\delta$ = 8.98 (d, $J$ = 5.0 Hz, 8H), 8.87 (d, $J$ = 5.0 Hz, 4H), 8.41 (m, 8H), 8.38 (d, $J$ = 5.0 Hz, 4H), 7.61 (s, 8H), 5.87 (s, 8H), 4.42 (s, 6H); $^{13}$C NMR (126 MHz, $CD_3CN$) $\delta$ = 150.1, 145.3, 144.1, 134.0, 134.0, 130.0, 130.0, 129.9, 127.2, 127.2, 127.1, 126.5, 125.4, 63.6; HRMS (ESI) $m/z$ calcd for $C_{48}H_{46}F_{30}N_6P_5$ $[M - PF_6]^+$ 1431.1988, found 1431.1982.

**S4·6PF$_6$/S5·22PF$_6$.** A solution of 1,4-bis(bromomethyl)benzene (1.1 g, 4.1 mmol) in dry MeCN (40 mL) was added over 10 h to a solution of **S3**·2$PF_6$ (6.25 g, 40 mmol) in dry MeCN (50 mL) while being heated under reflux. The mixture was heated for a further 120 h after the addition and then cooled to room temperature. The yellow precipitate was filtered off, washed with $Me_2CO$ and $Et_2O$, and finally purified by column chromatography ($SiO_2$) using 5% $NH_4PF_6$ (m/v) $Me_2CO$ solution as the eluent. The fractions were monitored by mass spectrometry and analytical HPLC. The pure fractions were combined, concentrated under vacuum, re-precipitated in $H_2O$, filtered off, and washed with $H_2O$ (50 mL), MeOH (20 mL), and finally $Et_2O$ (50 mL) to afford **S4**·4$PF_6$ (2.22 g, 30%) and **S5**·22$PF_6$ (1.52 g, 30%) as white solids. **S4**·4$PF_6$: $^1$H NMR (500 MHz, $CD_3CN$) $\delta$ = 8.97 (d, $J$ = 5.0 Hz, 8H), 8.87 (m, 8H), 8.41 (d, $J$ = 5.0 Hz, 8H), 8.36 (d, $J$ = 5.0 Hz, 4H), 7.82 (d, $J$ = 5.0 Hz, 4H), 7.61 (s, 4H), 7.60 (s, 8H), 5.87 (s, 8H), 5.81 (s, 4H); $^{13}$C NMR (126 MHz, $CD_3CN$) $\delta$ = 154.3, 150.7, 150.1, 145.3, 144.7, 140.9, 134.4, 134.0, 133.8, 130.0, 130.0, 129.8, 127.2, 126.0, 121.6, 117.0, 63.7, 63.6, 63.0; HRMS (ESI) $m/z$ calcd for $C_{64}H_{56}F_{30}N_8P_5$ $[M - PF_6]^+$ 1661.2831, found 1661.2811. **S5**·22$PF_6$: $^1$H NMR (500 MHz, $CD_3CN$) $\delta$ = 8.97 (d, $J$ = 5.0 Hz, 40H), 8.87 (m, 8H), 8.41 (d, $J$ = 5.0 Hz, 40H), 8.37 (d, $J$ = 5.0 Hz, 4H), 7.95 (d, $J$ = 5.0 Hz, 4H), 7.61 (m, 44H), 5.87 (s, 40H), 5.81 (s, 4H); $^{13}$C NMR (126 MHz, $CD_3CN$) $\delta$ = 150.1, 145.3, 134.0, 130.0, 129.9, 129.8, 127.2, 126.3, 63.6; HRMS (ESI) $m/z$ calcd for $C_{208}H_{184}N_{24}F_{114}P_{19}$ $[M - 3PF_6]^{3+}$ 1924.2796, found 1924.2642.

**4V·8PF$_6$.** MeI (251 mg, 1.85 mmol) was added dropwise to a solution of **S4**·6$PF_6$ (181 mg, 0.1 mmol) in DMF (3 mL) with stirring at room temperature. After addition, the mixture was heated to 90 °C for 72 h and cooled to room temperature, and then $Me_2CO$ was added to the solution. The resulting precipitate was filtered off, washed with $Me_2CO$, re-dissolved in $H_2O$, and re-precipitated by adding an excess of $NH_4PF_6$. The solid was filtered off and washed with $H_2O$, MeOH, and finally $Et_2O$ to afford **4V**·8$PF_6$ as a white solid (196 mg, 92%): $^1$H NMR (500 MHz, $CD_3CN$) $\delta$ = 8.98 (d, $J$ = 5.0 Hz, 12H), 8.87 (d, $J$ = 5.0 Hz, 4H), 8.41 (m, 12H), 8.38 (d, $J$ = 5.0 Hz, 4H), 7.61 (s, 12H), 5.87 (s, 12H), 4.42 (s, 6H); $^{13}$C NMR (126 MHz, $CD_3CN$) $\delta$ = 150.2, 149.1, 146.1, 145.3, 134.0, 130.0, 130.0, 127.2, 127.2, 126.5, 63.6. For crystal-growing experiments, **4V**·8$PF_6$ was converted to **4V**·8$SbF_6$. First, **4V**·8$PF_6$ was dissolved in MeCN and precipitated by adding an excess of TBACl. The solid was filtered off, washed with $Me_2CO$, re-dissolved in $H_2O$, and re-precipitated by adding an excess of $KSbF_6$ to afford **4V**·8$SbF_6$ as a white solid: HRMS (ESI) $m/z$ calcd for $C_{66}H_{62}F_{36}N_8Sb_6$ $[M - 2SbF_6]^{2+}$ 1189.9379, found 1189.9381.

**12V·24PF$_6$.** Dimethyl sulfate (300 mg, 2.38 mmol) was added to a solution of **S5**·22$PF_6$ (100 mg, 0.016 mmol) in DMF (3 mL). The mixture was heated to 90 °C for 5 days and cooled to room temperature, and then $Me_2CO$ was added to the solution. The resulting precipitate was filtered off, washed with $Me_2CO$, re-dissolved in $H_2O$, and re-precipitated by adding an excess of $NH_4PF_6$. The solid was filtered off and washed with $H_2O$, MeOH, and finally $Et_2O$ to afford **12V**·24$PF_6$ as a white solid (102 mg, 98%): $^1$H NMR (500 MHz, $CD_3CN$) $\delta$ = 8.98 (d, $J$ = 5.0 Hz, 44H), 8.87 (d, $J$ = 5.0 Hz, 4H), 8.42 (d, $J$ = 5.0 Hz, 44H), 8.38 (d, $J$ = 5.0 Hz, 4H), 7.62 (s, 44H), 5.87 (s, 44H), 4.42 (s, 6H); $^{13}$C NMR (126 MHz, $CD_3CN$) $\delta$ = 151.1, 146.3, 134.9, 130.9, 130.9, 128.2, 128.1, 127.4, 64.6, 30.5; HRMS (ESI) $m/z$ calcd for $C_{210}H_{190}N_{24}F_{126}P_{21}$ $[M - 3PF_6]^{3+}$ 2030.9371, found 2030.9343.

**Single-Crystal X-ray Diffraction (XRD).** A 0.2 mM MeCN solution of **3V**·6$PF_6$ was reduced by Zn dust to generate $\mathbf{3V}^{3(\bullet+)}$ before being filtered through a Pall syringe filter (pore size 0.45 $\mu$m) into VWR culture tubes (6 × 50 mm). The tubes were allowed to stand at room temperature in a closed scintillation vial containing $i$Pr$_2$O (3 mL). After 2 weeks, purple crystals of $[\mathbf{3V}^{3(\bullet+)}]_2$·6$PF_6$ appeared in the tubes, from which a rod-like crystal was picked out, mounted using oil (InfineumV8512) on a MiTeGew loop, transferred to the cold gas stream, and cooled by liquid $N_2$ on a Bruker APEX-II CCD detector with graphite-monochromated Cu K$\alpha$ radiation with MX optics. The superstructure was solved by direct methods and refined subsequently using the OLEX2 software. Crystallographic data are available free of charge from the Cambridge Crystallographic Data Centre (CCDC) using www.ccdc.cam.ac.uk/data_request/cif. *Crystal parameters for* $[\mathbf{3V}^{3(\bullet+)}]_2$·6$PF_6$: $C_{96}H_{92}F_{36}N_{12}P_6$, $M$ = 2283.63, crystal size 0.175 × 0.085 × 0.077 mm$^3$, orthorhombic, space group *Pnma*, $a$ = 25.5439(8), $b$ = 26.3802(8), $c$ = 38.3250(13) Å, $\alpha = \beta = \gamma$ = 90°, $V$ = 25825.4(1) Å$^3$, $T$ = 100(2) K, $Z$ = 6, $\rho_{calc}$ = 1.175. Of a total of 119860 reflections that were collected (4.066 ≤ 2Θ ≤ 130.284), 22396 were unique ($R_{int}$ = 0.0559, $R_{sigma}$ = 0.0396). Final $R_1(F^2 > 2\sigma F^2)$ = 0.1047, $wR_2$ = 0.3022. CCDC number: 1027540.

## RESULTS AND DISCUSSION

**Design Strategies.** On the basis of the ability of two $BIPY^{\bullet+}$ radical cations to form a stable dimer, we have designed and synthesized a series of redox-responsive foldamers based on oligobipyridinium chains,[8h,i] in which the structural folding resulting from radical-pairing interactions can be controlled reversibly by redox chemistry. By employing short, yet flexible, linkers to connect the multi-$BIPY^{2+}$ subunits together, the oligomers are extended in the fully oxidized state as a result of Coulombic repulsions between the positive charged $BIPY^{2+}$ subunits. On the other hand, upon reducing the oligomers, the resulting $BIPY^{\bullet+}$ radical cations curtail their occupation of space in order to interact with each other and consequently trigger the folding of the oligomers into stable (co)-conformations.


DOI: 10.1021/ja5111305
J. Am. Chem. Soc. 2015, 137, 876–885

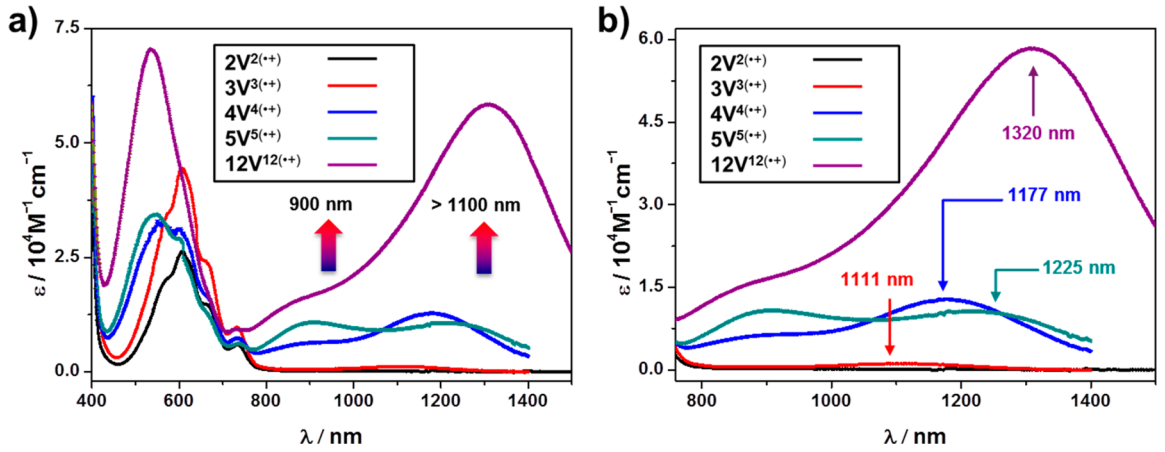


**Figure 2.** (a) Partial UV/Vis/NIR absorption spectra of $2V^{2(\bullet+)}$ (black), $3V^{3(\bullet+)}$ (red), $4V^{4(\bullet+)}$ (blue), $5V^{5(\bullet+)}$ (green), and $12V^{12(\bullet+)}$ (purple) recorded in MeCN at 298 K at the same concentration of 0.1 mM. (b) Enlargement of the spectra from 750 to 1500 nm, indicating a red-shift trend of the absorbance with increasing numbers of viologen subunits.

In order to implement the aforementioned design, we chose *p*-xylylene subunits as the linkers and synthesized a series (Figure 1) of homologous oligoviologens with different numbers of $BIPY^{2+}$ units—namely, two ($2V^{4+}$), three ($3V^{6+}$), four ($4V^{8+}$), five ($5V^{10+}$), and 12 ($12V^{24+}$) viologens. By employing UV/Vis/NIR spectroscopy and electrochemistry, in addition to X-ray crystallography, we have investigated the folding behavior of these oligoviologens in their radical cationic states, both in solution and in the solid state. It turns out that the folding is governed by both intra- and intermolecular radical−radical interactions between the $BIPY^{\bullet+}$ units, whose strengths are affected by the lengths of oligoviologen chains. The self-assembling properties of these radical cationic oligoviologens provide a unique example of molecular folding controlled by a redox stimulus.

**Synthetic Protocols.** On the basis of the structural similarities of the oligoviologen homologues (Figure 1), a general protocol for their syntheses has been established. Starting with 1,4-bis(bromomethyl)benzene and 4,4′-bipyridine, the oligoviologens were constructed (Schemes 1 and 2) through a sequence of nucleophilic substitutions followed by methylation steps. In order to prepare compound **3V**·$6PF_6$, the precursor **S1**·$2PF_6$ was mixed with 4,4′-bipyridine (molar ratio 1:10) in MeCN solution and heated under reflux for 3 days, giving in 80% yield the precursor **S2**·$4PF_6$, which was subsequently treated with MeI to afford compound **3V**·$6PF_6$. Likewise, in order to obtain compound **4V**·$8PF_6$, the precursor **S3**·$2PF_6$ was reacted with 1,4-bis(bromomethyl)benzene (molar ratio 10:1) in MeCN solution under reflux for 5 days. During the reaction, the nucleophilic substitution takes place to afford the crude products as white precipitates. Despite the fact that both the starting precursor $S3^{2+}$ and the products are insoluble in the presence of $Br^-$ ions, the larger oligoviologens, which contain more $BIPY^{2+}$ subunits and higher charges, are even more insoluble. Therefore, the crude products crash exclusively out of the solution as bromide salts, which can be filtered off easily so as to separate them from an excess of the starting precursors. **S4**·$6PF_6$ was obtained from the crude mixture by column chromatography, followed by counterion-exchange in 30% yield. Quite unexpectedly, in addition to **S4**·$6PF_6$, the larger homologue **S5**·$22PF_6$, was also isolated from the crude mixture in 30% yield, presumably as a result of a further reaction between **S4**·$6PF_6$ and 1,4-bis(bromomethyl)-benzene. **4V**·$8PF_6$ was obtained almost quantitatively by methylation of **S4**·$6PF_6$ with MeI in MeCN. Following the same procedures, however, an attempt to methylate **S5**·$22PF_6$ to give **12V**·$24PF_6$ with MeI was unsuccessful, probably on account of the fact that the nucleophilic $I^-$ ion cleaves the relatively long $S5^{22+}$ into shorter fragments, e.g., compounds with six and seven $BIPY^{2+}$ units. When MeI was replaced by $Me_2SO_4$ for the methylation of compound **S5**·$22PF_6$, the product **12V**·$24PF_6$ was obtained in over 90% yield. On account of the structural similarity of these five oligoviologens, their $^1H$ NMR spectra exhibit similar features (see SI, Figure S1). For example, the $\alpha$-protons on the $BIPY^{2+}$ subunits separate into two sets of peaks in all cases. One set of peaks corresponds to the $\alpha$-protons on the terminal methylated pyridinium rings at each end of the oligoviologens, and the other corresponds to the remainder of the $\alpha$-protons which resonate more downfield position because of the electron-withdrawing effect of the xylylene linkers. All the new compounds synthesized were characterized by $^1H$ and $^{13}C$ NMR spectroscopies, as well as by HRMS.

**Spectroscopic Investigations.** The folding of the oligoviologens was first investigated by UV/Vis/NIR spectroscopy. In the fully oxidized forms of the oligoviologens, the high electrostatic repulsion between $BIPY^{2+}$ subunits, along with their similar $\pi$-electron-deficient nature, inhibits aggregation between charged oligoviologens. Following reduction of the oligoviologens $2V^{4+}$, $3V^{6+}$, $4V^{8+}$, $5V^{10+}$, and $12V^{24+}$ to the corresponding radical cationic states $2V^{2(\bullet+)}$, $3V^{3(\bullet+)}$, $4V^{4(\bullet+)}$, $5V^{5(\bullet+)}$, and $12V^{12(\bullet+)}$ with zinc dust, the absorption spectra of 0.1 mM MeCN solutions of these radical cationic oligoviologens[25] were obtained (Figure 2) at room temperature. The spectra (Figure 2a) exhibit the typical absorption band[17] for the $BIPY^{\bullet+}$ radical cationic species, centered around 600 nm. Moreover, two distinct absorption bands at 900 and above 1000 nm can be distinguished (Figure 2b) in the spectra of $4V^{4(\bullet+)}$, $5V^{5(\bullet+)}$, and $12\ V^{12(\bullet+)}$. The band centered on 900 nm can be ascribed[18a] to the formation of radical−radical dimers $[BIPY^{\bullet+}]_2$, while the one above 1000 nm can be assigned[18a] to the formation of trisradical complexes involving three $BIPY^{\bullet+}$ units. Although all of the five radical cationic oligoviologens, including $2V^{2(\bullet+)}$, exhibit (see SI, Figure S6) absorption bands above 1000 nm, only three of them—namely, $4V^{4(\bullet+)}$, $5V^{5(\bullet+)}$, and $12V^{12(\bullet+)}$—absorb significantly at 900 nm. The spectro-


DOI: 10.1021/ja5111305
J. Am. Chem. Soc. 2015, 137, 876−885

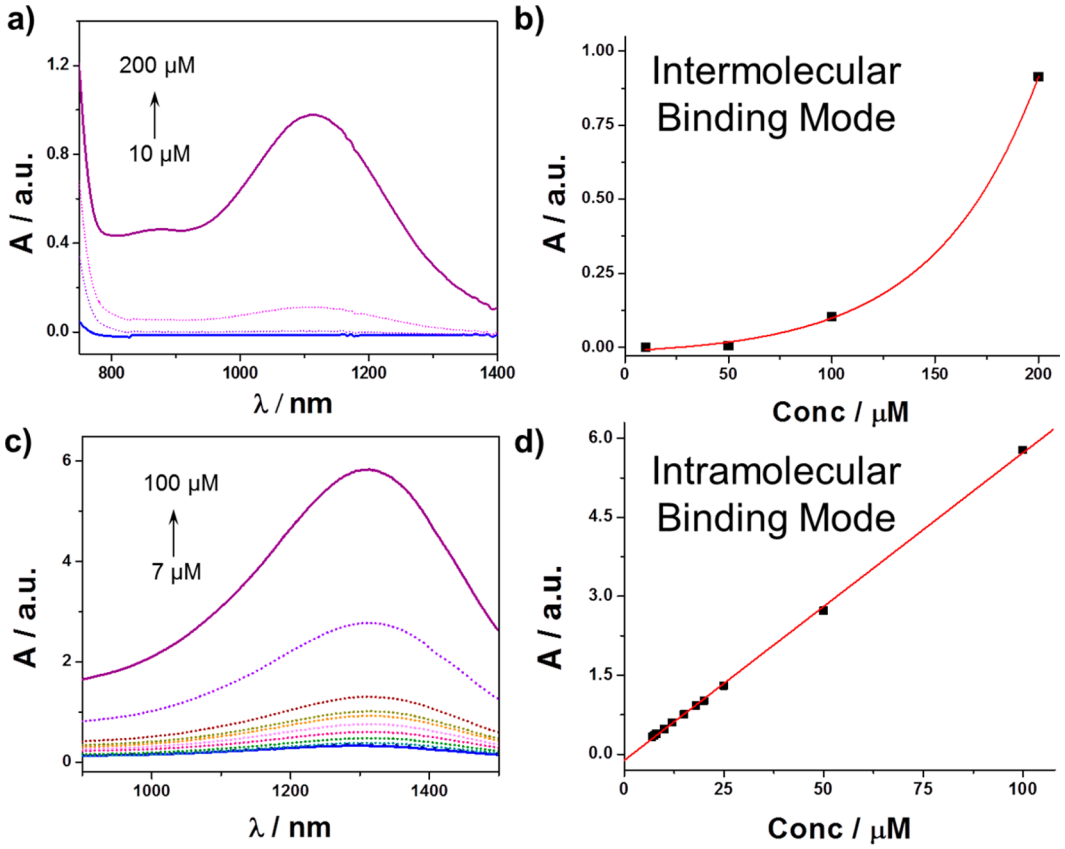


**Figure 3.** (a) UV/Vis/NIR spectra of $\mathbf{3V}^{3(\bullet+)}$ recorded over a range of different concentrations. (b) Dependence of the intensity of the band at 1111 nm on concentration. The nonlinear change of the intensity can be attributed to intermolecular interactions. (c) UV/Vis/NIR spectra of $\mathbf{12V}^{12(\bullet+)}$ recorded over a range of different concentrations. (d) Dependence of the intensity of the band at 1320 nm on concentration. The linear dependence of the intensity with the concentration can be ascribed to the intramolecular interactions.

scopic behavior of these oligoviologens suggests that the interactions become more complex with increasing numbers of $BIPY^{\bullet+}$ units.

In order to investigate the nature of the interactions involved in these oligoviologens, concentration-dependent absorption spectra in the NIR region were obtained. The spectroscopic features of the five oligoviologens display different concentration-dependent behavior despite their similar structural characteristics. The concentration-dependent absorption spectra of the two extreme cases—namely, $\mathbf{3V}^{3(\bullet+)}$ and $\mathbf{12V}^{12(\bullet+)}$—are compared in Figure 3. Upon increasing the concentration of $\mathbf{3V}^{3(\bullet+)}$ from 10 to 200 $\mu$M, an absorption band (Figure 3a) centered on 1111 nm emerges. The nonlinear relationship (Figure 3b) of the intensities of this absorption band with respect to increasing concentration indicates the formation of intermolecular radical–radical interactions between $\mathbf{3V}^{3(\bullet+)}$ units. This type of interaction can be achieved in the form of intertwining folded complexes involving two or more $\mathbf{3V}^{3(\bullet+)}$ units, in which the $BIPY^{\bullet+}$ units assume a specific (co)-conformation in order to maximize[26] the stabilization obtained from the formation of trisradical complexes. By contrast, in the case (Figure 3c) of $\mathbf{12V}^{12(\bullet+)}$, a linear correlation between the absorption intensities and the concentrations is observed (Figure 3d). This observation suggests that the interactions between $BIPY^{\bullet+}$ subunits in $\mathbf{12V}^{12(\bullet+)}$ are controlled chiefly by intramolecular interactions and hence are independent of changes in concentration.

More intricate folding mechanisms can be ascribed to the mid-length homologues, which combine features of both the shorter and longer oligoviologens. For example, in the case of $\mathbf{5V}^{5(\bullet+)}$, although the intensities of absorption bands centered on 900 and 1225 nm become simultaneously stronger with increasing concentration, the absorption-concentration relationship is linear for the former band, whereas it is nonlinear for the latter one (see SI, Figure S4). This observation demonstrates (Figure 4) that both intra- and intermolecular radical–radical interactions are involved[18a] in determining the folding behavior of $\mathbf{5V}^{5(\bullet+)}$. While the absorption band centered on 1225 nm results from the intermolecular radical–radical interactions, the intramolecular interactions resulting from the dimerization of two $BIPY^{\bullet+}$ subunits within one $\mathbf{5V}^{5(\bullet+)}$ give rise to the absorption at 900 nm. More evidence has been obtained by performing UV/Vis/NIR spectroscopy in a MeCN/DMF mixed solvent (3:7, v/v) (see SI, Figure S5).

When comparing the wavelengths of the absorption bands from $\mathbf{2V}^{2(\bullet+)}$ to $\mathbf{12V}^{12(\bullet+)}$, although there are no large shifts in the radical dimer absorption bands,[18a,27] a significant red-shift from 1050 to 1320 nm is observed (Figure 2b) in the absorption bands corresponding to trisradical complexation.[28] This observation suggests that, in addition to (i) intramolecular interactions being favored over intermolecular ones, as well as (ii) trisradical complexation being favored over radical dimerization, the longer oligoviologens display higher stabilities in the case of their radical cationic species as a consequence of the extended $\pi$–$\pi$ stacking systems sustained by the $BIPY^{\bullet+}$ subunits. In other words, the relative energy level of the radical cationic states is lower.[27]



DOI: 10.1021/ja5111305
J. Am. Chem. Soc. 2015, 137, 876–885

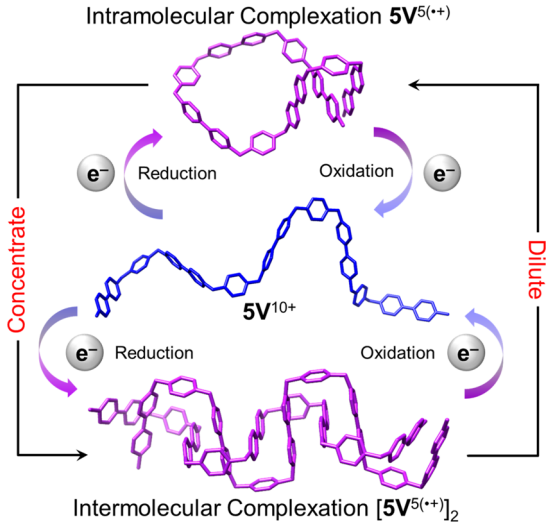


**Figure 4.** Schematic illustration of the possible switching process operating between the simulated inter- and intramolecular binding states of $\mathbf{5V}^{5(\bullet+)}$ under redox stimulus.

**Electrochemical Studies.** Cyclic voltammetry (CV) provides further insight into the mechanism of radical dimerization in the oligoviologens. Upon scanning the potential in a negative direction, all five oligoviologens show (Figure 5) one reversible redox peak in the vicinity of −320 mV, which can be ascribed[15] to a one-electron reduction of each $BIPY^{2+}$ unit to a $BIPY^{\bullet+}$ radical cation. The reduction potentials for the different oligoviologens display a significantly positive shift from −370 mV for $\mathbf{2V}^{4+}$ to −280 mV for $\mathbf{12V}^{24+}$. This positive shift in the potential with an increasing number of $BIPY^{2+}$ units reflects more negative $\Delta G$ values for the reduction of the longer oligoviologens. On the one hand, the decreased electron density, on account of the increasing Coulombic repulsion between proximal $BIPY^{2+}$ units in the longer oligoviologens, increases the energy of the oxidized states. On the other hand, once reduced to their radical cationic states, the Coulombic repulsion within the oligoviologens are replaced by the attractive radical−radical interactions. Since longer oligoviologens are capable of providing more significant radical stabilization by means of intramolecular radical−radical interactions, their reduced states have a relatively lower energy level. As a result, the longer oligoviologens are more easily reduced to their radical cationic states than the shorter ones.

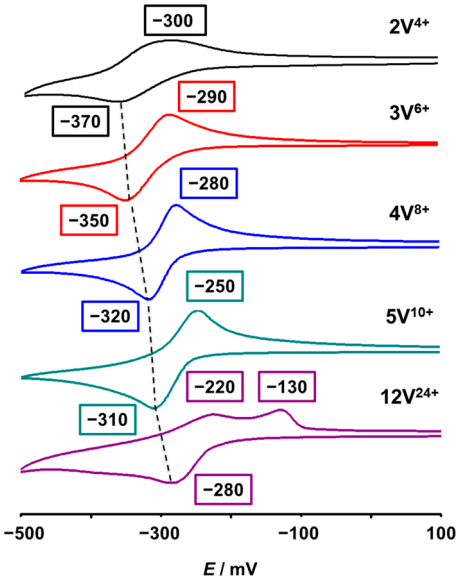


**Figure 5.** Cyclic voltammograms of five oligoviologens. The redox peaks, which correspond to the one-electron reduction of each $BIPY^{2+}$ unit, show a shift toward positive potential with increasing numbers of $BIPY^{2+}$ units, indicating that the stability of the radical cation is enhanced. The additional peak at −130 mV in the case of $\mathbf{12V}^{24+}$ can be attributed to intramolecular radical dimer formation resulting from one-electron oxidation of the intramolecular trisradical complex. A glassy carbon working electrode, a platinum counter electrode, and a Ag/AgCl reference electrode were used in the characterization of 0.1 mM MeCN solutions of the oligoviologens at 298 K with 0.1 M $TBAPF_6$ serving as the electrolyte. A scan rate of 200 $mV{\cdot}s^{-1}$ was used in all the analyses.

In contrast to its shorter counterparts, which all undergo simultaneously oxidation upon scanning the potential in a positive direction, the CV profile of the longest $\mathbf{12V}^{24+}$ displays two oxidation peaks at a scan rate of 200 $mV{\cdot}s^{-1}$. On being reduced at −280 mV, $\mathbf{12V}^{24+}$ receives 12 electrons to give the radical cationic species $\mathbf{12V}^{12(\bullet+)}$, a condition that induces the formation of intramolecular trisradical complexes between $BIPY^{\bullet+}$ subunits. Upon oxidation, the first peak centered at −220 mV can be assigned to the oxidation of the unpaired $BIPY^{\bullet+}$ subunits in the trisradical complexes, which are more weakly engaged in radical−radical interactions, while the second oxidation peak, shifted by 90 mV toward more positive potential, can be assigned to the simultaneous two-electron oxidation of the $BIPY^{\bullet+}$ dimers to afford the $\mathbf{12V}^{24+}$ state. This observation is in agreement with the results obtained from UV/Vis/NIR spectra and confirms the higher stability of the folded $\mathbf{12V}^{12(\bullet+)}$ as a result of intramolecular radical−radical interactions in comparison with the shorter oligoviologens.

**X-ray Crystallography.** In order to investigate in more detail the structural changes that can occur during the folding of oligoviologens upon reduction of the $BIPY^{2+}$ subunits to the $BIPY^{\bullet+}$ radical cations, an X-ray crystallographic investigation was carried out on $\mathbf{3V}^{3(\bullet+)}$. Slow vapor diffusion of $i\mathrm{Pr}_2\mathrm{O}$ into a $\mathbf{3V}^{3(\bullet+)}$ solution in MeCN (100 $\mu$M), which was generated by reduction with Zn dust, provided single crystals suitable for X-ray diffraction analysis. The solid-state superstructure reveals (Figure 6a) the formation of a repeating unit—namely, the hexaradical hexacationic complex $[\mathbf{3V}^{3(\bullet+)}]_2$—that is composed of two identical $\mathbf{3V}^{3(\bullet+)}$ which are intertwined with each other in order to maximize[26] the intermolecular radical−radical interactions. This packing corresponds to the superstructure we proposed exists in solution on the basis of spectroscopic investigations! In particular, the six $BIPY^{\bullet+}$ subunits present in the $[\mathbf{3V}^{3(\bullet+)}]_2$ dimer, three from each $\mathbf{3V}^{3(\bullet+)}$ monomer, stack alternately along the *a* axis, forming an intertwined hexaradical hexacationic repeating unit. This folded structure, which allows the maximum amount of radical−radical pimerization to take place, plays a crucial role in stabilizing the solid-state superstructure of $\mathbf{3V}^{3(\bullet+)}$. Interestingly, the centroid-to-centroid distances between adjacent $BIPY^{\bullet+}$ radical cationic subunits within the $[\mathbf{3V}^{3(\bullet+)}]_2$ dimer are approximately 3.22 Å at the center of dimer while they are slightly shorter (3.18 Å) at the ends, leaving the $[\mathbf{3V}^{3(\bullet+)}]_2$ dimer stacked more loosely in the center and more tightly at the ends.

Despite the relatively high flexibility of oligoviologen $\mathbf{3V}^{3(\bullet+)}$ compared with a more rigid structure, such as the $\mathbf{CBPQT}^{2(\bullet+)}$, the $BIPY^{\bullet+}$ subunits stack in an highly ordered manner. For


DOI: 10.1021/ja5111305
J. Am. Chem. Soc. 2015, 137, 876−885

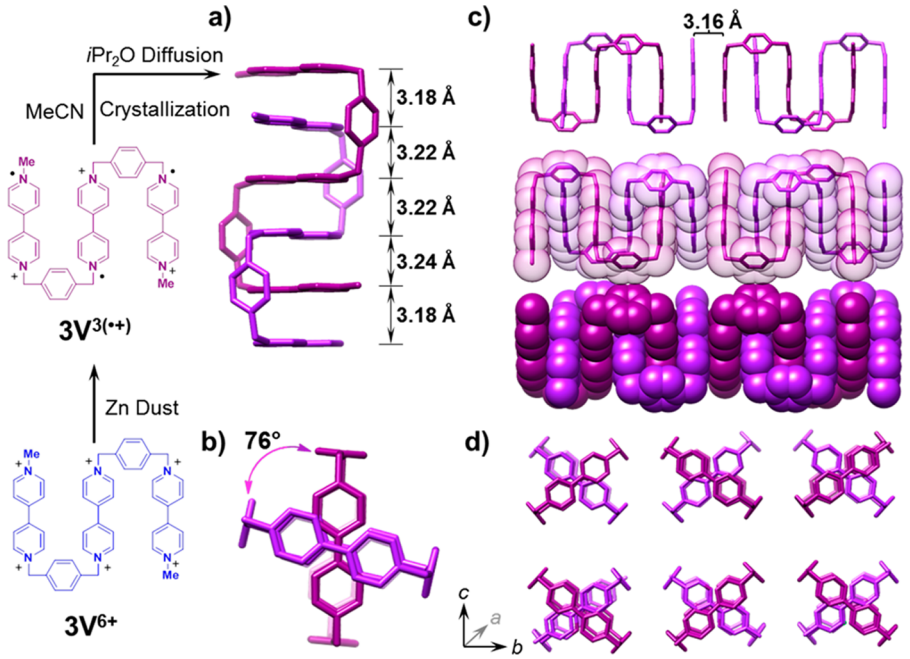


**Figure 6.** Solid-state superstructures of $\mathbf{3V}^{3(\bullet+)}$ obtained by single-crystal X-ray crystallography. (a) Wireframe representation of the $\mathbf{3V}^{3(\bullet+)}$ where two $\mathbf{3V}^{3(\bullet+)}$ oligomers intertwine as a result of radical−radical interactions. (b) Wireframe representation of the $\mathbf{3V}^{3(\bullet+)}$ from a side-on perspective, illustrating the angle between two $\mathbf{3V}^{3(\bullet+)}$ units in the dimer superstructure. (c) Wireframe and space-filling representations along the *a*-axis of the long-range packing order of the radical cationic species $\mathbf{3V}^{3(\bullet+)}$, which forms a continuous radical−radical $\pi\cdots\pi$ stack. (d) Side-on view of the unit cell of the radical cationic species $\mathbf{3V}^{3(\bullet+)}$ determined by X-ray crystallography, revealing the superstructure. The $PF_6^-$ counterions and MeCN solvent molecules have been omitted for the sake of clarity.

example, the angle (Figure 6b) between any two adjacent $BIPY^{\bullet+}$ subunits of the $[\mathbf{3V}^{3(\bullet+)}]_2$ dimer in the *b*−*c* plane is 76°. This deviation from orthogonality, which maximizes[29] the $\pi$-overlap area between two adjacent $BIPY^{\bullet+}$ radical cations, shares features that are similar to the solid-state superstructure[23b] of the 1:1 inclusion complex between $\mathbf{MV}^{\bullet+}$ and $\mathbf{CBPQT}^{2(\bullet+)}$. The extended superstructure reveals (Figure 6c) an infinite columnar stacking of $BIPY^{\bullet+}$ units through radical−radical pairing interactions, with adjacent dimer complexes aligned in register, i.e., with the same angle offset of 76° between adjacently stacked complexes. A centroid-to-centroid distance between the $BIPY^{\bullet+}$ radical cationic subunits of adjacent hexaradical hexacationic complexes—which is subject to less control by the rigidity of $\mathbf{3V}^{3(\bullet+)}$—was found to be 3.16 Å, i.e., a distance which is even shorter than the inner complex distance.

The continuous radical cationic stack displayed by $\mathbf{3V}^{3(\bullet+)}$, which is similar to (i) those reported by Kochi[30] in 1990 for the $\mathbf{MV}^{\bullet+}$ radical cation in the solid state and also (ii) the solid-state superstructure[23b] of $\mathbf{MV}^{\bullet+}\subset\mathbf{CBPQT}^{2(\bullet+)}$, is reminiscent of polymeric crystalline lattice superstructures reported previously.[31] The interplanar distances between two adjacent $BIPY^{\bullet+}$ subunits, both within the hexaradical hexacationic repeating units (3.18−3.24 Å) and between adjacent repeating units (3.16 Å), are less when compared with those (3.25 Å) present in the $\mathbf{MV}^{\bullet+}\subset\mathbf{CBPQT}^{2(\bullet+)}$ inclusion complex. This contraction in $\pi$−$\pi$ stacking distances can be attributed to (i) the fact that the acyclic $\mathbf{3V}^{3(\bullet+)}$ is more flexible than the cyclic $\mathbf{CBPQT}^{2(\bullet+)}$, allowing the $BIPY^{\bullet+}$ subunits to come closer together when they stack, and (ii) the cooperative effect of radical−radical interactions between two $\mathbf{3V}^{3(\bullet+)}$ units in the $[\mathbf{3V}^{3(\bullet+)}]_2$ dimers.

**Computational Studies.** The role played by the intra- and intermolecular interactions in the binding mode and the (co)-conformations of the oligoviologens has also been explored computationally. Here we proposed possible geometries for the different binding modes that we anticipate would maximize the interactions between the radicals, and then we used DFT methods[32] to optimize these geometries and obtain binding energies. In the case of intermolecular binding between two $\mathbf{3V}^{3(\bullet+)}$ units, these DFT calculations (Figure 7) show that the contact between the two radical cationic $BIPY^{\bullet+}$ units is maximized in the intertwined dimer, a result supported by the solid-state superstructure. On the other hand, a hairpin-like conformation is adopted in the cases of $\mathbf{4V}^{4(\bullet+)}$ and $\mathbf{5V}^{5(\bullet+)}$ secondary structures, which is prevented from forming in the case of short oligoviologens, simply because the strain to bring two terminal $BIPY^{(\bullet+)}$ units together is far too large.

Furthermore, we investigated the folding of the oligoviologens by calculating the reaction Gibbs free energy, which we separate into the enthalpic and entropic contributions. The enthalpic component, derived from the DFT calculations of the interaction between radical cation $BIPY^{\bullet+}$ subunits in the oligoviologens, is controlled by (i) the strength of spin-pairing (bonding) of two adjacent $BIPY^{(\bullet+)}$ subunits and (ii) the electrostatic repulsion between all positively charged $BIPY^{(\bullet+)}$ subunits in the presence of solvent and counterions in solution. These two factors are included in our DFT calculation and solvation model. For the intermolecular binding, the longer oligoviologens exhibit a larger enthalpy change as more $BIPY^{(\bullet+)}$ subunits are involved in the $\pi$−$\pi$ stacking system. In the case of intramolecular binding, the enthalpy change exhibits a similar trend, presumably because increasing molecular flexibility in the longer oligoviologens facilitates stronger interactions between $BIPY^{(\bullet+)}$ subunits. The entropic component is estimated by observing the change of the number of degree of freedom (DOF) based on the facts in the process of


DOI: 10.1021/ja5111305
J. Am. Chem. Soc. 2015, 137, 876−885

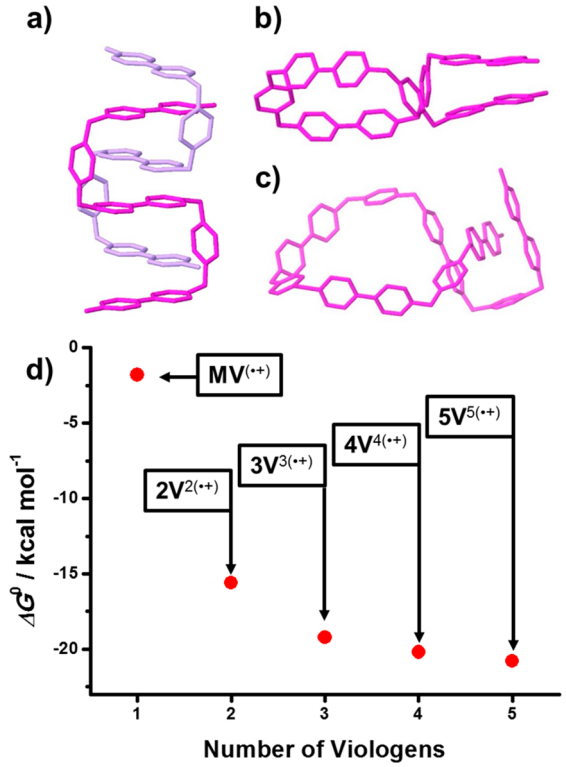


**Figure 7.** Simulated (co)-conformations of oligoviologens in different binding modes. (a) Two $3V^{3(\bullet+)}$ intertwining with each other in an intermolecular binding mode. Two terminal $BIPY^{\bullet+}$ subunits interact in the cases of (b) $4V^{4(\bullet+)}$ and (c) $5V^{5(\bullet+)}$ in the intramolecular binding mode. (d) The trend in the $\Delta G^0$ values varies with the lengths of the oligoviologens in their intermolecular binding mode, demonstrating that this energy value saturates when the number of viologen subunits exceeds three.

folding: (i) the intermolecular binding brings two oligoviologens together, converting three translational and three rotational DOFs (high entropy) to six low-frequency vibrational modes, and (ii) the pimerization of each $BIPY^{(\bullet+)}$ pair blocks the rotation about the C−C bond between methylene and paired $BIPY^{(\bullet+)}$ subunits, in addition to (iii) the formation of the hairpin-like intramolecular complex also restricts some of such C−C bond rotations. The estimated entropy change (Table 1) grows more negative with increasing numbers of $BIPY^{\bullet+}$ subunits in the case of both the inter- and intramolecular binding modes, across the series of $MV^{\bullet+}$, $2V^{2(\bullet+)}$, $3V^{3(\bullet+)}$, $4V^{4(\bullet+)}$, and $5V^{5(\bullet+)}$. As a consequence, the overall change of $\Delta G^0$ values increases and then saturates (Figure 7d) as the length of oligoviologen increases. From the calculated $\Delta G^0$ values, the contribution of the intra- and intermolecular interactions involved in the folding of oligoviologens can be estimated. For $4V^{4(\bullet+)}$, we estimate that an intertwined dimer is 16.0 kcal·mol$^{-1}$ more stable[40] than two $4V^{4(\bullet+)}$ with intramolecular binding, whereas for $5V^{5(\bullet+)}$ this energy difference drops[41] to 5.4 kcal·mol$^{-1}$. Thus, this simple model reveals the insight that strain from the intermolecular binding is compensated by the smaller entropy penalty incurred and further diminished as the chain length grows. Therefore, for longer oligoviologens, the intramolecular binding is favored.

## CONCLUSIONS

We have prepared a homologous series of oligoviologens with different numbers of $BIPY^{2+}$ subunits. UV/Vis/NIR spectroscopic and electrochemical investigations have indicated that the oligoviologens are folded as a consequence of radical−radical interactions under reducing conditions in solution. A solid-state superstructure reveals that two $3V^{3(\bullet+)}$ strands form an intertwining folded dimer which continues to pack in an infinite stack[30] as a result of intermolecular radical−radical interactions. At low concentrations, the shortest of the oligoviologens ($2V^{2(\bullet+)}$) show neither strong intra- nor intermolecular interactions between its $BIPY^{\bullet+}$ units as a result of the limited conformational space it can adopt and its weak radical−radical interaction affinity. However, the slightly longer oligoviologen ($3V^{3(\bullet+)}$) forms complexes driven by intermolecular radical−radical interactions. On increasing the number of $BIPY^{\bullet+}$ units even further, the intramolecular radical−radical interactions become important, which gradually overcome the intermolecular interactions to become the dominant factor in controlling the folding of the oligoviologens because of their increased flexibility until $12V^{12(\bullet+)}$ is reached in the extreme case. In a nutshell, the secondary structures of the foldamers are controlled by intra- and intermolecular interactions, both of which are dependent on the lengths and concentrations of their

**Table 1. Summary of the Thermodynamic Data Obtained from Calculations Describing the Intramolecular and Intermolecular Radical−Radical Interactions-Induced Folding Processes**

| | $\Delta S^0$ (cal·K$^{-1}$·mol$^{-1}$) | | | | |
|---|---|---|---|---|---|
| oligoviologens | translational[a] | rotational[b] | overall $T\Delta S^0$ (kcal·mol$^{-1}$)[c] | $\Delta H^0$ (kcal·mol$^{-1}$) | $\Delta G^0$ (kcal·mol$^{-1}$) |
| | | | Intermolecular Interactions | | |
| $1V^{(\bullet+)}$ | −17.3 | −6.2 | −7.0 | −8.8 | −1.8 |
| $2V^{2(\bullet+)}$ | −18.6 | −22.8 | −12.3 | −27.9 | −15.6 |
| $3V^{3(\bullet+)}$ | −19.3 | −39.4 | −17.5 | −36.7 | −19.2 |
| $4V^{4(\bullet+)}$ | −19.7 | −55.9 | −22.5 | −42.7 | −20.2 |
| $5V^{5(\bullet+)}$ | −20.1 | −72.5 | −27.6 | −48.4 | −20.8 |
| | | | Intramolecular Interactions | | |
| $4V^{4(\bullet+)}$ | | −14.5 | −4.3 | −6.4 | −2.1 |
| $5V^{5(\bullet+)}$ | | −22.8 | −6.8 | −14.5 | −7.7 |

[a]To estimate the entropy change of reaction, the translational entropy of each species in solution is approximated[36] to half of its gas-phase value[37] so that the entropy penalty[38] for two oligoviologen molecules to form an intertwined dimer can be obtained. [b]For the calculation of the rotational entropy change, a 2.07 cal·K$^{-1}$·mol$^{-1}$ per rotor is employed.[39] Each rotational degree of freedom of the whole molecule that turns into low-frequency vibrations during the dimerization is also approximated as a frustrated rotor. [c]$T$ = 298 K.



DOI: 10.1021/ja5111305
J. Am. Chem. Soc. 2015, 137, 876−885

components in solution. This behavior is reminiscent of the trends for secondary structural elements present in the more complex biomacromolecules.

## ■ ASSOCIATED CONTENT

### Supporting Information

Detailed synthetic procedures and characterization (NMR, HRMS, and HPLC) data for all compounds; spectroscopic (NMR and UV/Vis/NIR) and electrochemical (CV) studies for $\mathbf{2V}^{2(\bullet+)}$, $\mathbf{4V}^{4(\bullet+)}$, and $\mathbf{5V}^{5(\bullet+)}$; computational analysis for $\mathbf{2V}^{2(\bullet+)}$, $\mathbf{3V}^{3(\bullet+)}$, $\mathbf{4V}^{4(\bullet+)}$, and $\mathbf{5V}^{5(\bullet+)}$; and X-ray crystallographic analysis data (CIF) for $[\mathbf{3V}^{3(\bullet+)}]_2 \cdot 6PF_6$. This material is available free of charge via the Internet at http://pubs.acs.org.

## ■ AUTHOR INFORMATION


### Corresponding Author

stoddart@northwestern.edu


### Notes

The authors declare no competing financial interest.

## ■ ACKNOWLEDGMENTS

This research is part (Project 34-945) of the Joint Center of Excellence in Integrated Nano-Systems (JCIN) at King Abdul-Aziz City for Science and Technology (KACST) and Northwestern University (NU). The authors thank both KACST and NU for their continued support of this research. The computational studies (W.-G.L., W.A.G.) were supported by NSF (EFRI-ODISSEI 1332411)

## ■ REFERENCES


(1) (a) Lehn, J.-M. *Supramolecular Chemistry—Concepts and Perspectives*; Wiley-VCH: Weinheim, 1995. (b) Hill, D. J.; Mio, M. J.; Prince, R. B.; Hughes, T. S.; Moore, J. S. *Chem. Rev.* **2001**, *101*, 3893. (c) Schenning, A. P. H. J.; Meijer, E. W. *Chem. Commun.* **2005**, 3245. (d) Salonen, L. M.; Ellermann, M.; Diederich, F. *Angew. Chem., Int. Ed.* **2011**, *50*, 4808.

(2) (a) Hill, T. L. *J. Am. Chem. Soc.* **1956**, *78*, 3330. (b) Creighton, T. E. *Proteins: Structures and Molecular Principles*, 2nd ed.; Freeman: New York, 1993.

(3) (a) Saenger, W. *Principles of Nucleic Acid Structure*; Springer-Verlag: New York, 1984. (b) Strobel, S. A.; Doudna, J. A. *Trends Biochem. Sci.* **1997**, *22*, 262. (c) Vasudev, P. G.; Chatterjee, S.; Shamala, N.; Balaram, P. *Chem. Rev.* **2011**, *111*, 657.

(4) (a) Sharma, G. V.; Reddy, K. R.; Krishna, P. R.; Sankar, A. R.; Narsimulu, K.; Kumar, S. K.; Jayaprakash, P.; Jagannadh, B.; Kunwar, A. C. *J. Am. Chem. Soc.* **2003**, *125*, 13670. (b) Hayen, A.; Schmitt, M. A.; Ngassa, F. N.; Thomasson, K. A.; Gellman, S. H. *Angew. Chem., Int. Ed.* **2004**, *43*, 505. (c) Mándity, I. M.; Wéber, E.; Martinek, T. A.; Olajos, G.; Tóth, G. K.; Vass, E.; Fülöp, F. *Angew. Chem., Int. Ed.* **2009**, *48*, 2171. (d) Hetényi, A.; Tóth, G. K.; Somlai, C.; Vass, E.; Martinek, T. A.; Fülöp, F. *Chem.—Eur. J.* **2009**, *15*, 10736. (e) Claudon, P.; Violette, A.; Lamour, K.; Decossas, M.; Fournel, S.; Heurtault, B.; Godet, J.; Mély, Y.; Jamart-Grégoire, B.; Averlant-Petit, M.-C.; Briand, J.-P.; Duportail, G.; Monteil, H.; Guichard, G. *Angew. Chem., Int. Ed.* **2010**, *49*, 333. (f) Guo, L.; Almeida, A. M.; Zhang, W.; Reidenbach, A. G.; Choi, S. H.; Guzei, I. A.; Gellman, S. H. *J. Am. Chem. Soc.* **2010**, *132*, 7868. (g) Kudo, M.; Maurizot, V.; Kauffmann, B.; Tanatani, A.; Huc, I. *J. Am. Chem. Soc.* **2013**, *135*, 9628.

(5) (a) Cantor, C. R.; Schimmel, P. R. *Biophysical Chemistry: I. The Conformation of Biological Macromolecules*; W. H. Freeman and Co.: San Francisco, 1980. (b) Goodman, C. M.; Choi, S.; Shandler, S. *Nature Chem. Biol.* **2007**, *3*, 252. (c) James, W. H.; Muller, C. W.; Buchanan, E. G.; Nix, M. G. D.; Guo, L.; Roskop, L.; Gordon, M. S.; Slipchenko, L.V.; Gellman, S. H.; Zwier, T. S. *J. Am. Chem. Soc.* **2009**, *131*, 14243.

(6) (a) Daniels, D. S.; Petersson, E. J.; Qiu, J. X.; Schepartz, A. *J. Am. Chem. Soc.* **2007**, *129*, 1532. (b) Horne, W. S.; Price, J. L.; Keck, J. L.; Gellman, S. H. *J. Am. Chem. Soc.* **2007**, *129*, 4178.

(7) (a) Stigers, K. D.; Soth, M. J.; Nowick, J. S. *Curr. Opin. Chem. Biol.* **1999**, *3*, 714. (b) Park, J.-S.; Lee, H.-S.; Lai, J. R.; Kim, B. M.; Gellman, S. H. *J. Am. Chem. Soc.* **2003**, *125*, 8539. (c) Ernst, J. T.; Becerril, J.; Park, H. S.; Yin, H.; Hamilton, A. D. *Angew. Chem., Int. Ed.* **2003**, *42*, 535. (d) Moriuchi, T.; Hirao, T. *Chem. Soc. Rev.* **2004**, *33*, 294. (e) Cai, W.; Wang, G. T.; Du, P.; Wang, R. X.; Jiang, X. K.; Li, Z. T. *J. Am. Chem. Soc.* **2008**, *130*, 13450. (f) Guo, L.; Chi, Y. G.; Almeida, A. M.; Guzei, I. A.; Parker, B. K.; Gellman, S. H. *J. Am. Chem. Soc.* **2009**, *131*, 16018. (g) Baptiste, B.; Godde, F.; Huc, I. *ChemBioChem* **2009**, *10*, 1765. (h) Yashima, E.; Maeda, K.; Iida, H.; Furusho, Y.; Nagai, K. *Chem. Rev.* **2009**, *109*, 6102. (i) Kwon, S.; Jeon, A.; Yoo, S. H.; Chung, I. S.; Lee, H. S. *Angew. Chem., Int. Ed.* **2010**, *49*, 8232. (j) Kim, J.; Kwon, S.; Kim, S. H.; Lee, C. K.; Lee, J. H.; Cho, S. J.; Lee, H. S.; Ihee, H. *J. Am. Chem. Soc.* **2012**, *134*, 20573. (k) Cheng, P. N.; Pham, J. D.; Nowick, J. S. *J. Am. Chem. Soc.* **2013**, *135*, 5477.

(8) (a) Gellman, S. H. *Acc. Chem. Res.* **1998**, *31*, 173. (b) Berl, V.; Huc, I.; Khoury, R.; Krische, M. J.; Lehn, J.-M. *Nature* **2000**, *407*, 720. (c) Hill, D. J.; Mio, M. J.; Prince, R. B.; Hughes, T. S.; Moore, J. S. *Chem. Rev.* **2001**, *101*, 3893. (d) Sessler, J.; Jayawickramarajah, J. *Chem. Commun.* **2005**, *15*, 1939. (e) Stone, M. T.; Heemstra, J. M.; Moore, J. S. *Acc. Chem. Res.* **2006**, *39*, 11. (f) Hecht, S.; Huc, I. *Foldamers: Structure, Properties and Applications*; Wiley-VCH: Weinheim, 2007. (g) Guichard, G.; Huc, I. *Chem. Commun.* **2011**, *47*, 5933. (h) Zhu, Z.; Li, H.; Liu, Z.; Lei, J.; Zhang, H.; Botros, Y. Y.; Stern, C. L.; Sarjeant, A. A.; Stoddart, J. F.; Colquhoun, H. M. *Angew. Chem., Int. Ed.* **2012**, *51*, 7231. (i) Bruns, C. J.; Stoddart, J. F. *Adv. Polym. Sci.* **2013**, *261*, 271.

(9) (a) Lokey, R. S.; Iverson, B. L. *Nature* **1995**, *375*, 303. (b) Lokey, R. S.; Kwok, Y.; Guelev, V.; Pursell, C. J.; Hurley, L. H.; Iverson, B. L. *J. Am. Chem. Soc.* **1997**, *119*, 7202. (c) Horne, W. S.; Ashkenasy, N.; Ghadiri, M. R. *Chem.—Eur. J.* **2005**, *11*, 1137. (d) Horne, W. S.; Gellman, S. H. *Acc. Chem. Res.* **2008**, *41*, 1399. (e) Saraogi, I.; Hamilton, A. D. *Chem. Soc. Rev.* **2009**, *38*, 1726. (f) Juwarker, H.; Jeong, K. S. *Chem. Soc. Rev.* **2010**, *39*, 3664. (g) Iavicoli, P.; Xu, H.; Feldborg, L. N.; Linares, M.; Paradinas, M.; Stafstrom, S.; Ocal, C.; Nieto-Ortega, B. L.; Casado, J.; Navarrete, J. T. L.; Lazzaroni, R.; De Feyter, S.; Amabilino, D. B. *J. Am. Chem. Soc.* **2010**, *132*, 9350. (h) Zhang, D. W.; Zhao, X.; Hou, J. L.; Li, Z. T. *Chem. Rev.* **2012**, *112*, 5271. (i) Martinek, T. A.; Fülöp, F. *Chem. Soc. Rev.* **2012**, *41*, 687. (j) Martinez, C. R.; Iverson, B. L. *Chem. Sci.* **2012**, *3*, 2191. (k) Gong, H.-Y.; Rambo, B.; Lynch, V. M.; Keller, K.; Sessler, J. L. *J. Am. Chem. Soc.* **2013**, *135*, 6330.

(10) (a) Cubberley, M. S.; Iverson, B. L. *J. Am. Chem. Soc.* **2001**, *123*, 7560. (b) Gabriel, G. J.; Iverson, B. L. *J. Am. Chem. Soc.* **2002**, *124*, 15174. (c) Marcos Ramos, A.; Meskers, S. C. J.; Beckers, E. H. A.; Prince, R. B.; Brunsveld, L.; Janssen, R. A. J. *J. Am. Chem. Soc.* **2004**, *126*, 9630. (d) Cai, W.; Wang, G. T.; Xu, Y. X.; Jiang, X. K.; Li, Z. T. *J. Am. Chem. Soc.* **2008**, *130*, 6936. (e) Wolffs, M.; Delsuc, N.; Veldman, D.; Nguyen, V. A.; Williams, R. M.; Meskers, S. C.; Janssen, R. A.; Huc, I.; Schenning, A. P. *J. Am. Chem. Soc.* **2009**, *131*, 4819. (f) Martinez, A.; Guy, L.; Dutasta, J.-P. *J. Am. Chem. Soc.* **2010**, *132*, 16733.

(11) (a) Martinez de Ilarduya, A.; Alemán, C.; García-Alvarez, M.; López-Carrasquero, F.; Muñoz-Guerra, S. *Macromolecules* **1999**, *32*, 3257. (b) Nguyen, J. Q.; Iverson, B. L. *J. Am. Chem. Soc.* **1999**, *121*, 2639. (c) Fujiki, M. *J. Organomet. Chem.* **2003**, *685*, 15.

(12) (a) Berl, V.; Huc, I.; Khoury, R. G.; Lehn, J.-M. *Chem.—Eur. J.* **2001**, *7*, 2798. (b) Dolain, C.; Maurizot, V.; Huc, I. *Angew. Chem., Int. Ed.* **2003**, *42*, 2738. (c) Kolomiets, E.; Berl, V.; Lehn, J.-M. *Chem.—Eur. J.* **2007**, *13*, 5466. (d) Hu, H.-Y.; Xiang, J.-F.; Yang, Y.; Chen, C.-F. *Org. Lett.* **2008**, *10*, 1275. (e) Stadler, A. M.; Lehn, J. M. P. *J. Am. Chem. Soc.* **2014**, *136*, 3400.

(13) (a) Nicoll, A. J.; Miller, D. J.; Futterer, K.; Ravelli, R.; Allemann, R. K. *J. Am. Chem. Soc.* **2006**, *128*, 9187. (b) Zhao, Y.; Zhong, Z. Q. *J. Am. Chem. Soc.* **2006**, *128*, 9988. (c) Delsuc, N.; Hutin, M.; Campbell, V. E.; Kauffmann, B.; Nitschke, J. R.; Huc, I. *Chem.—Eur. J.* **2008**, *14*,




DOI: 10.1021/ja5111305
*J. Am. Chem. Soc.* 2015, 137, 876–885

7140. (d) Suk, J. M.; Naidu, V. R.; Liu, X. F.; Lah, M. S.; Jeonet, K. S. *J. Am. Chem. Soc.* **2011**, *133*, 13938. (e) Hua, Y. R.; Liu, Y.; Chen, C. H.; Flood, A. H. *J. Am. Chem. Soc.* **2013**, *135*, 14401.
(14) (a) Khan, A.; Kaiser, C.; Hecht, S. *Angew. Chem., Int. Ed.* **2006**, *45*, 1878. (b) Hua, Y. R.; Flood, A. H. *J. Am. Chem. Soc.* **2010**, *132*, 12838. (c) Wang, Y.; Bie, F.; Jiang, H. *Org. Lett.* **2010**, *12*, 3630. (d) Yu, Z. L.; Hecht, S. *Chem.—Eur. J.* **2012**, *18*, 10519.
(15) Kosower, E. M.; Cotter, J. L. *J. Am. Chem. Soc.* **1964**, *86*, 5524.
(16) Hünig, S. *Pure Appl. Chem.* **1967**, *15*, 109.
(17) (a) Kosower, E. M.; Hajdu, J. *J. Am. Chem. Soc.* **1971**, *93*, 2534. (b) Geuder, W.; Hünig, S.; Suchy, A. *Angew. Chem., Int. Ed. Engl.* **1983**, *22*, 489. (c) Monk, P. M. S. *The Viologens: Physicochemical Properties, Synthesis and Applications of the Salts of 4,4′-Bipyridine*; Wiley: New York, 1998.
(18) (a) Geuder, W.; Hunig, S.; Suchy, A. *Tetrahedron* **1986**, *42*, 1665. (b) Monk, P. M. S.; Hodgkinson, N. M.; Ramzan, S. A. *Dyes Pigments* **1999**, *43*, 207.
(19) (a) Iordache, A.; Oltean, M.; Milet, A.; Thomas, F.; Baptiste, B.; Saint-Aman, E.; Bucher, C. *J. Am. Chem. Soc.* **2012**, *134*, 2653. (b) Fahrenbach, A. C.; Sampath, S.; Late, D. J.; Barnes, J. C.; Kleinman, S. L.; Valley, N.; Hartlieb, K. J.; Liu, Z.; Dravid, V. P.; Schatz, G. C.; Van Duyne, R. P.; Stoddart, J. F. *ACS Nano* **2012**, *6*, 9964. (c) Bergamini, G.; Fermi, A.; Marchini, M.; Locritani, M.; Credi, A.; Venturi, M.; Negri, F.; Ceroni, P.; Baroncini, M. *Chem.—Eur. J.* **2012**, *18*, 7648. (d) Iehl, J.; Frasconi, M.; Jacquot de Rouville, H.-P.; Renaud, N.; Dyar, S. M.; Strutt, N. L.; Carmieli, R.; Wasielewski, M. R.; Ratner, M. A.; Nierengarten, J.-F.; Stoddart, J. F. *Chem. Sci.* **2013**, *4*, 1462.
(20) (a) Jeon, W. S.; Kim, H.-J.; Lee, C.; Kim, K. *Chem. Commun.* **2002**, 1828. (b) Trabolsi, A.; Hmadeh, M.; Khashab, N. M.; Friedman, D. C.; Belowich, M. E.; Humbert, N.; Elhabiri, M.; Khatib, H. A.; Albrecht-Gary, A.-M.; Stoddart, J. F. *New J. Chem.* **2009**, *33*, 254. (c) Ho Ko, Y.; Kim, Y.; Kim, H.; Kim, K. *Chem.—Asian J.* **2011**, *6*, 2. (d) Gao, C.; Silvi, S.; Ma, X.; Tian, H.; Venturi, M.; Credi, A. *Chem. Commun.* **2012**, *48*, 7577.
(21) (a) Atherton, S. J.; Tsukahara, K.; Wilkins, R. G. *J. Am. Chem. Soc.* **1986**, *108*, 3380. (b) Imabayashi, S.-I.; Kitamura, N.; Tazuke, S.; Tokuda, K. *J. Electroanal. Chem.* **1988**, *243*, 143. (c) Kannappan, R.; Bucher, C.; Saint-Aman, E.; Moutet, J.-C.; Milet, A.; Oltean, M.; Métay, E.; Pellet-Rostaing, S.; Lemaire, M.; Chaix, C. *New J. Chem.* **2010**, *34*, 1373. (d) Iordache, A.; Retegan, M.; Thomas, F.; Royal, G.; Saint-Aman, E.; Bucher, C. *Chem.—Eur. J.* **2012**, *18*, 7648.
(22) (a) Marchioni, F.; Venturi, M.; Ceroni, P.; Balzani, V.; Belohradsky, M.; Elizarov, A. M.; Tseng, H.-R.; Stoddart, J. F. *Chem.—Eur. J.* **2004**, *10*, 6361. (b) Ronconi, C. M.; Stoddart, J. F.; Balzani, V.; Baroncini, M.; Ceroni, P.; Giansante, C.; Venturi, M. *Chem.—Eur. J.* **2008**, *14*, 8365.
(23) (a) Trabolsi, A.; Khashab, N.; Fahrenbach, A. C.; Friedman, D. C.; Colvin, M. T.; Coti, K. K.; Benitez, D.; Tkatchouk, E.; Olsen, J. C.; Belowich, M. E.; Carmielli, R.; Khatib, H. A.; Goddard, W. A.; Wasielewski, M. R.; Stoddart, J. F. *Nat. Chem.* **2010**, *2*, 42. (b) Fahrenbach, A. C.; Barnes, J. C.; Lanfranchi, D. A.; Li, H.; Coskun, A.; Gassensmith, J. J.; Liu, Z.; Benitez, D.; Trabolsi, A.; Goddard, W. A.; Elhabiri, M.; Stoddart, J. F. *J. Am. Chem. Soc.* **2012**, *134*, 3061.
(24) (a) Li, H.; Fahrenbach, A. C.; Dey, S. K.; Basu, S.; Trabolsi, A.; Zhu, Z. X.; Botros, Y. Y.; Stoddart, J. F. *Angew. Chem., Int. Ed.* **2010**, *49*, 8260. (b) Li, H.; Cheng, C. Y.; McGonigal, P. R.; Fahrenbach, A. C.; Frasconi, M.; Liu, W. G.; Zhu, Z. X.; Zhao, Y. L.; Ke, C. F.; Lei, J. Y.; Young, R. M.; Dyar, S. M.; Co, D. T.; Yang, Y. W.; Botros, Y. Y.; Goddard, W. A.; Wasielewski, M. R.; Astumian, R. D.; Stoddart, J. F. *J. Am. Chem. Soc.* **2013**, *135*, 18609. (c) Barnes, J. C.; Fahrenbach, A. C.; Cao, D.; Dyar, S. M.; Frasconi, M.; Giesener, M. A.; Benitez, D.; Tkatchouk, E.; Chernyashevskyy, O.; Shin, W. H.; Li, H.; Sampath, S.; Stern, C. L.; Sarjeant, A. A.; Hartlieb, K. J.; Liu, Z.; Carmieli, R.; Botros, Y. Y.; Choi, J. W.; Slawin, A. M. Z.; Ketterson, J. B.; Wasielewski, M. R.; Goddard, W. A.; Stoddart, J. F. *Science* **2013**, *339*, 429. (d) Bruns, C. J.; Frasconi, M.; Iehl, J.; Hartlieb, K. J.; Schneebeli, S. T.; Cheng, C.; Stupp, S. I.; Stoddart, J. F. *J. Am. Chem. Soc.* **2014**, *136*, 4714. (e) Cheng, C.; McGonigal, P. R.; Liu, W.-G.; Li, H.; Vermeulen, N. A.; Ke, C.; Frasconi, M.; Stern, C. L.; Goddard, W. A.; Stoddart, J. F. *J. Am. Chem. Soc.* **2014**, *136*, 14702.
(25) Endo, T.; Ageishi, K.; Okawara, M. *J. Org. Chem.* **1986**, *51*, 4309.
(26) Kramer, R.; Lehn, J. M.; Marquis-Rigault, A. *Proc. Natl. Acad. Sci. U.S.A.* **1993**, *90*, 5394.
(27) Lu, J. M.; Rosokha, S.V.; Kochi, J. K. *J. Am. Chem. Soc.* **2003**, *125*, 12161.
(28) Sun, D. L.; Rosokha, S.V.; Lindeman, S.V.; Kochi, J. K. *J. Am. Chem. Soc.* **2003**, *125*, 15950.
(29) Hunter, C. A.; Sanders, J. K. M. *J. Am. Chem. Soc.* **1990**, *112*, 5525.
(30) Bockman, T. M.; Kochi, J. K. *J. Org. Chem.* **1990**, *55*, 4127.
(31) (a) Colquhoun, H. M.; Williams, D. J. *Acc. Chem. Res.* **2000**, *33*, 189. (b) Colquhoun, H. M.; Aldred, P. L.; Zhu, Z. X.; Williams, D. J. *Macromolecules* **2003**, *36*, 6416. (c) Makin, O. S.; Sikorski, P.; Serpell, L. C. *J. Appl. Crystallogr.* **2007**, *40*, 966. (d) Arosio, P.; Moreno, M.; Famulari, A.; Raos, G.; Catellani, M.; Meille, S.V. *Chem. Mater.* **2009**, *21*, 78. (e) Lebeau, C.; Guillou, H.; Tessier, C.; Brisson, J. *Polymer* **2011**, *52*, 4083.
(32) The geometries were optimized with density functional theory (DFT) at the level of M06-L/6-31G** in the Poisson−Boltzmann solvation model[33] for MeCN ($\varepsilon$ = 37.5 and $R_0$ = 2.18 Å) with Jaguar 7.7.[34] The single-point energy was refined at the M06/6-311++G** level.[35]
(33) Tannor, D. J.; Marten, B.; Murphy, R.; Friesner, R. A.; Sitkoff, D.; Nicholls, A.; Ringnalda, M.; Goddard, W. A.; Honig, B. *J. Am. Chem. Soc.* **1994**, *116*, 11875.
(34) *Jaguar*, version 7.7; Schrodinger, LLC: New York, 2007.
(35) Zhao, Y.; Truhlar, D. G. *Theor. Chem. Acc.* **2008**, *120*, 215.
(36) For the entropy part, it is not practical to calculate analytically with DFT due to the size of oligoviologens.
(37) Wertz, D. H. *J. Am. Chem. Soc.* **1980**, *102*, 5316.
(38) Page, M. I.; Jencks, W. P. *Proc. Natl. Acad. Sci. U.S.A.* **1971**, *68*, 1678.
(39) Searle, M. S.; Williams, D. H. *J. Am. Chem. Soc.* **1992**, *114*, 10690.
(40) On the basis of the $\Delta G^0$ values summarized in Table 1, this energy difference is obtained from the equation $\Delta(\Delta G^0) = (-2.1\ \text{kcal·mol}^{-1} \times 2) - (-20.2\ \text{kcal·mol}^{-1})$, which is +16.0 kcal·mol$^{-1}$.
(41) On the basis of the $\Delta G^0$ values summarized in Table 1, this energy difference is obtained from the equation $\Delta(\Delta G^0) = (-7.7\ \text{kcal·mol}^{-1} \times 2) - (-20.8\ \text{kcal·mol}^{-1})$, which is +5.4 kcal·mol$^{-1}$.


DOI: 10.1021/ja5111305
*J. Am. Chem. Soc.* 2015, 137, 876−885